Hindawi
International Journal of Antennas and Propagation
Volume 2017, Article ID 1513038, 15 pages
https://doi.org/10.1155/2017/1513038

Research Article

Channel Measurements and Modeling at 6 GHz in the Tunnel Environments for 5G Wireless Systems

Shuang-de Li,[1] Yuan-jian Liu,[1] Le-ke Lin,[2] Zhong Sheng,[1] Xiang-chen Sun,[1] Zhi-peng Chen,[1] and Xiao-jun Zhang[1]

[1]*College of Electronic and Optical Engineering, Nanjing University of Posts and Telecommunications, Nanjing, Jiangsu 210003, China*
[2]*National Key Laboratory of Electromagnetic Environment, China Research Institute of Radio Wave Propagation, Qingdao, Shandong 266107, China*

Correspondence should be addressed to Shuang-de Li; 1014020807@njupt.edu.cn

Received 14 May 2017; Revised 8 August 2017; Accepted 8 October 2017; Published 10 December 2017

Academic Editor: Larbi Talbi

Propagation measurements of wireless channels performed in the tunnel environments at 6 GHz are presented in this paper. Propagation characteristics are simulated and analyzed based on the method of shooting and bouncing ray tracing/image (SBR/IM). A good agreement is achieved between the measured results and simulated results, so the correctness of SBR/IM method has been validated. The measured results and simulated results are analyzed in terms of path loss models, received power, root mean square (RMS) delay spread, Ricean K-factor, and angle of arrival (AOA). The omnidirectional path loss models are characterized based on close-in (CI) free-space reference distance model and the alpha-beta-gamma (ABG) model. Path loss exponents (PLEs) are 1.50–1.74 in line-of-sight (LOS) scenarios and 2.18–2.20 in non-line-of-sight (NLOS) scenarios. Results show that CI model with the reference distance of 1 m provides more accuracy and stability in tunnel scenarios. The RMS delay spread values vary between 2.77 ns and 18.76 ns. Specially, the Poisson distribution best fits the measured data of RMS delay spreads for LOS scenarios and the Gaussian distribution best fits the measured data of RMS delay spreads for NLOS scenarios. Moreover, the normal distribution provides good fits to the Ricean K-factor. The analysis of the abovementioned results from channel measurements and simulations may be utilized for the design of wireless communications of future 5G radio systems at 6 GHz.

1. Introduction

The next generation (5G) of wireless communications will use systems operating from 500 MHz to 300 GHz [1, 2]. The 3 GHz–30 GHz spectrum is defined as the super high frequency (SHF) band, while 30–300 GHz spectrum is assigned to the extremely high frequency (EHF) or millimeter-wave band (mmWave) [3]. Because radio waves in the SHF and EHF bands share similar propagation characteristics, the 3–300 GHz spectrum, with wavelengths ranging from 1 mm–100 mm, can be referred to as the EHF bands [4, 5]. The EHF bands will be a key component, which can deliver multigigabit-per-second transmission throughputs for various multimedia services for 5G radio systems [6, 7]. Thus, fundamental knowledge of the EHF channel propagation characteristics including accurate and reliable channel models is vital for developing 5G wireless communication systems.

Many extensive EHF wireless channel measurement campaigns have been investigated for different scenarios in multiple outdoor and indoor environments, yielding empirically based path loss models and delay dispersion properties. Some research projects, such as METIS [8], NYU WIRELESS [1, 5, 9, 10], MiWEBA [11], and mmMagic [12], have been developing 5G mmWave channel models which are mainly aimed at the outdoor cellular propagation channel and indoor office scenarios including street-canyon, shopping malls, and stadium scenarios. Millimeter-wave propagation characteristics in the laboratory environment are analyzed at the 28 GHz and 82 GHz [13]. A vehicle

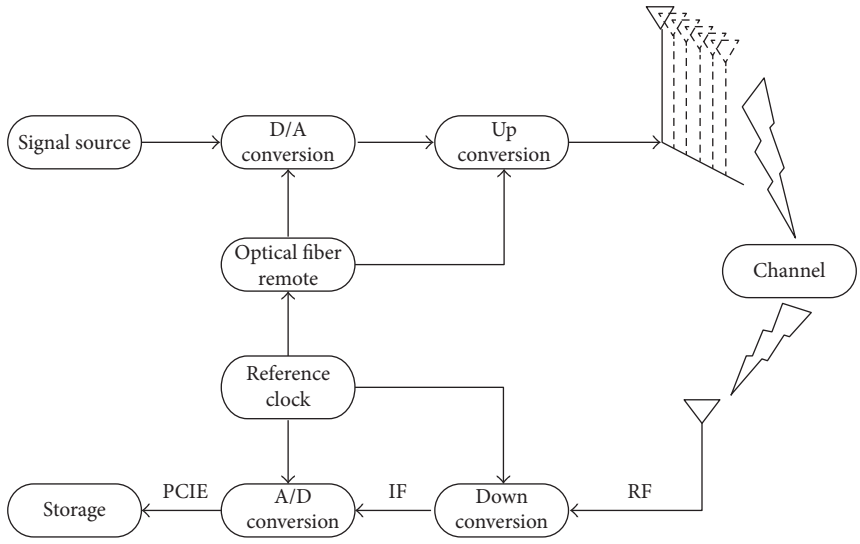

Figure 1: Overview of the measurement setup.

channel measurement is conducted for different antenna placements and antenna patterns at 55–65 GHz [14]. Moreover, multiple wireless channel sounding campaigns have been presented in the literature for access environments above 3GHz, for example, at 5.3 GHz [15], 10 GHz [16], 11 GHz [17], 15 GHz [18], 28 GHz [5, 13, 18–21], 32 GHz [22], 38 GHz and 73 GHz [1, 5, 23–26], 60 GHz and 70 GHz [16, 27–30], 83.5 GHz [31], and 110 GHz [32].

Although a large number of channel-measured results can provide reliable channel model, the expense of high-precision measurement equipment is very high and the number of observation points is limited in measurement campaigns, which are both great challenges for channel sounding. As an another approach, the shooting and bouncing ray-tracing/image (SBR/IM) method [33] is an effective method, which can extend the sparse empirical datasets and can be utilized to investigate the propagation characteristics of EHF bands. Also, it is able to capture multipath components in time-varying wireless channels and can prove the accuracy and effectiveness of the proposed channel model by comparing simulated channel model with the actual measured channel model. In this paper, we verify that the simulated results provide good agreement with measured results over all the measured paths, as we compared simulations with measurements in the same tunnel environment and distance ranges for verification.

Despite many measurement campaigns were conducted up to now, there are still omitted environments and frequency bands, which require to be intensively investigated. Hence, extensive actual channel measurements and simulations should be performed for various scenarios and significant frequency bands. By analyzing the measured results and simulated results, a standardized channel model should be proposed. The contribution of this paper is fivefold. First of all, channel measurements and simulations in the tunnel environments are performed and analyzed at 6 GHz, which have not been detailed in previous work. Therefore, propagation characteristics are analyzed at 6 GHz in the tunnel environment. Second, the omnidirectional path loss models are characterized based on close-in (CI) free-space reference distance model and the alpha-beta-gamma (ABG) model. In addition, the comprehensive parameter table of path loss models including measured results and simulated results for all scenarios is given. Third, the statistical analysis of the RMS delay spread for tunnel scenarios is described using measurement datasets. The fourth part of the contribution is to investigate the different distribution models based on the cumulative distribution functions (CDF) in terms of the parameters of received power, Ricean K-factor, and angle of arrival (AOA). Finally, some important angle of arrival is extracted based on the subtractive clustering algorithm.

The rest of the paper is organized as follows. The measurement setup and environments are described in Section 2. The results and analysis of path loss models are presented in Section 3. Specially, the parameters of received power, Ricean K-factor, and angle of arrival (AOA) are evaluated in Section 3. Finally, conclusions are drawn in Section 4.

2. Measurement Setup and Environments

2.1. Measurement Setup and Procedure. Measurements were conducted in the frequency domain in which the channel impulse responses (CIRs) were measured and recorded. Figure 1 illustrates an overview of the channel measurement setup. The height of the transmission antenna is 1.8 m, while the height of the receiver antenna is 1.6 m above the floor in the tunnel environments. Table 1 shows the 6 GHz channel sounding system parameters, and more detailed information of the channel sounder and calibration method can be found in [34].

2.2. Environment Description. Two tunnel propagation measurement campaigns were conducted in the tunnel chamber of Beijing Jiaotong University (BJTU) in Beijing, China, in

Table 1: Channel sounding system parameters used at 6 GHz.

Parameters	Value
Carrier frequency	6 GHz
RF bandwidth	100 MHz
Excitation sequence	Multicarrier signal
Subcarrier number	2560
Effective subcarrier number	2048
TX/RX antenna	Omnidirectional/omnidirectional
Transmission power	10 dBm
TX/RX antenna gains	20 dBi/20 dBi
TX/RX antenna height	1.8 m/1.6 m
TX-RX synchronization	Supported

two different scenarios as shown in Figures 2(a) and 2(b), respectively. The receiver antenna moves along a straight line. The first to be taken (LOS-1 measurement) was performed at a sampling distance of 1 m. The transmitter (TX1) was placed almost at one end of a long tunnel, while the receiver (RX) was moving along a LOS route (A-B, 19 m), which corresponds to 20 samples as shown in Figure 2(c). The second to be taken (LOS-2 measurement) was also taken at a sampling distance of 1 m. The transmitter (TX2) was placed at the corner, while the receiver (RX) was moving along a LOS route (C-D, 11 m), which corresponds to 12 samples as shown in Figure 2(c). Moreover, the third to be taken (NLOS measurement), the transmitter (TX1) was also placed almost at one end of a long tunnel, while the receiver (RX) was moving along a route (A-B-C-D, 30 m), which corresponds to 31 samples as shown in Figure 2(c). The last to be taken (LOS-3 measurement) was taken at a sampling distance of 0.5 m. The transmitter (TX) was indicated in the tunnel scenario, while the receiver (RX) was moving along a LOS route (A-B, 8 m), which corresponds to 17 samples as shown in Figure 2(d). At each receiver location, measurements were acquired using a circular track with 8 equally spaced local area measurement points separated by 45° increments. The radius of the circular track yielded 3λ and 2λ separation distance between consecutive points along the circular track in tunnel 1 and tunnel 2 scenarios, respectively. Note that in the measurement, no one was moving in the tunnel, so as to eliminate the influence of moving persons.

2.3. Ray-Tracing Simulations. The shooting and bouncing ray-tracing/image (SBR/IM) method is developed to deal with the radio wave propagation for complex environment. It can track all the triangular ray tubes bouncing with high accuracy and computational efficiency. If the RX is within a ray tube, the ray tube will have contribution to the received field at RX and the equivalent source (image) can be determined. So SBR/IM method is an effective method which can be used to predict the propagation characteristics at 6 GHz.

The ray-tracing simulation performs the method of SBR/IM using the software tool, Wireless InSite [35]. In our simulation settings, the ray-tracer accounts for up to 6 reflections, 2 penetrations, and 1 diffraction for each ray. The material properties are frequency-dependent, and the parameters of dielectric constant ε_r and conductivity σ in this paper are estimated for the 6 GHz spectrum band based on the material properties in different bands [36–39]. The buildings are assumed to be concrete with the dielectric constant $\varepsilon_r = 6.94$ and $\sigma = 0.73S/m$, respectively. For each simulated RX point, a discrete equivalent baseband CIR was composed from the simulated rays based on their complex amplitude and delay spread. Furthermore, the ray-tracing simulation performed for the purpose of validation is presented for proper comparison and validation of simulated results and empirical results. This is further discussed in Section 3.

3. Channel Models and Statistical Analysis

3.1. Path Loss Models. The path loss is a significant parameter which can be applicable to describe the large-scale effects of the propagation channel [40]. In this work, two kinds of path loss models are considered based on the measurements and simulations, namely, the close-in (CI) free-space reference distance path loss model [41, 42] and the alpha-beta-gamma (ABG) path loss model [9].

Two well-known models are used to develop omnidirectional path loss models in this paper. First of all, the equation for the CI model is given by

$$\mathrm{PL}^{\mathrm{CI}}(f,d)[\mathrm{dB}] = 20\log_{10}\left(\frac{4\pi f d_0}{c}\right)[\mathrm{dB}] + 10n\log_{10}\left(\frac{d}{d_0}\right) + X_\sigma^{\mathrm{CI}}, \quad (1)$$

where d_0 is the close-in free-space reference distance, f is the carrier frequency in GHz, c is the speed of light, n denotes the path loss exponent (PLE), d is the distance between transmitter and receiver, and X_σ^{CI} is a zero-mean Gaussian random variable with a standard deviation σ in dB (shadowing effect). The minimum mean square error (MMSE) is used to calculate PLE and standard deviation. The physical interpretation of $n = 1$ is a guided wave in one plane, $n = 2$corresponds to a free-space path loss, and $n = 4$ corresponds to a situation, where low antenna heights cause the first Fresnel zone to be obstructed [15].

The ABG model is another famous model which can be used to discuss the frequency dependence of path loss. It can be defined as [24]

$$\mathrm{PL}^{\mathrm{ABG}}(f,d)[\mathrm{dB}] = 10\alpha\log_{10}\left(\frac{d}{1\ \mathrm{m}}\right) + \beta + 10\gamma\log_{10}\left(\frac{f}{1\ \mathrm{GHz}}\right) + X_\sigma^{\mathrm{ABG}}, \quad (2)$$

where $\mathrm{PL}^{\mathrm{ABG}}(f,d)$ denotes the path loss in dB over frequency and distance; α and $\gamma$are coefficients showing the dependence of path loss on distance and frequency, respectively; β is an optimized offset value for path loss in dB; and X_σ^{ABG} is a zero-mean Gaussian random variable with a standard deviation σ in dB derived from MMSE closed-form optimization.

(a)

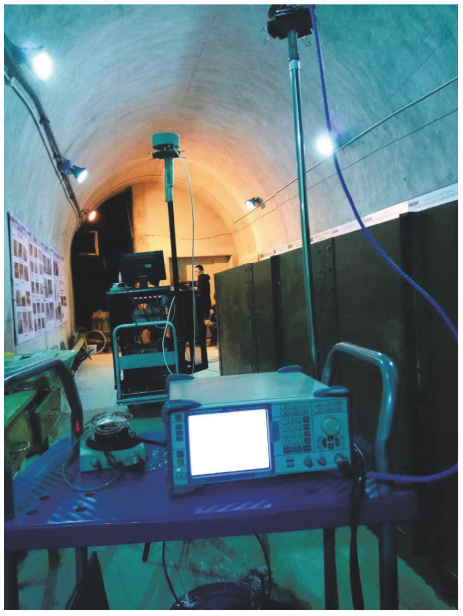

(b)

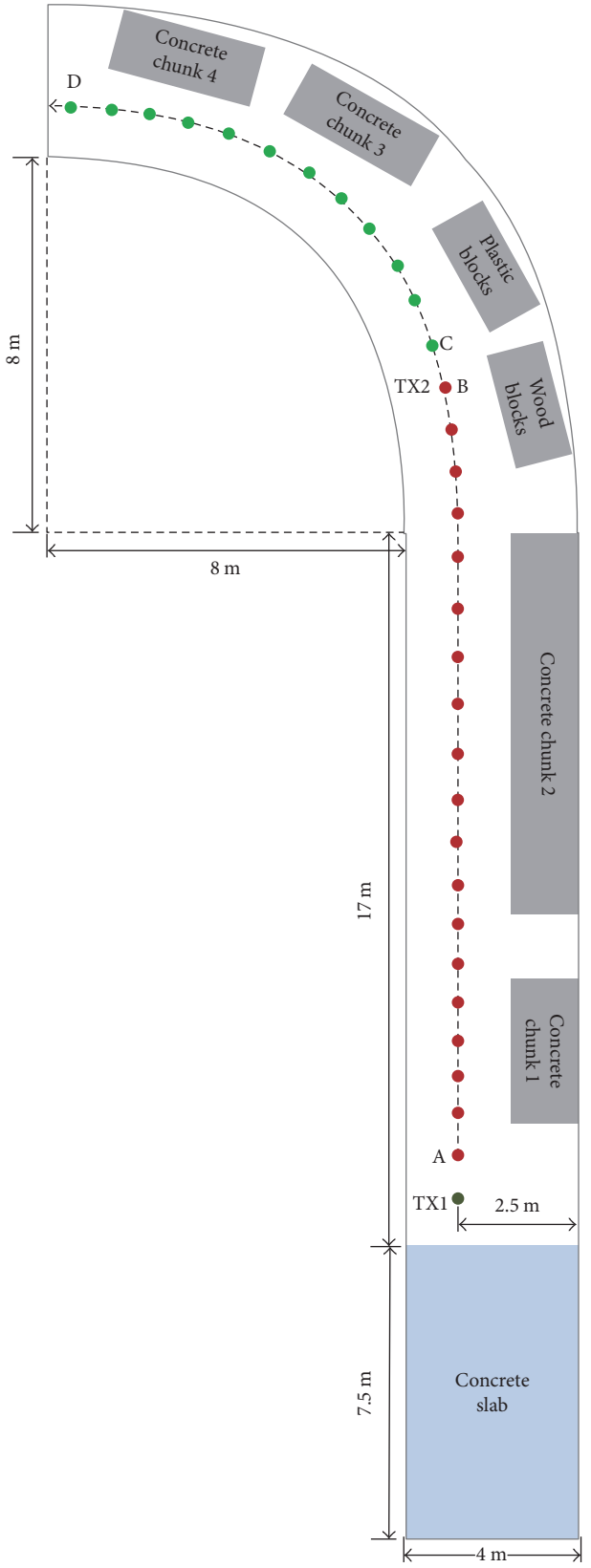

(c)

Figure 2: Continued.

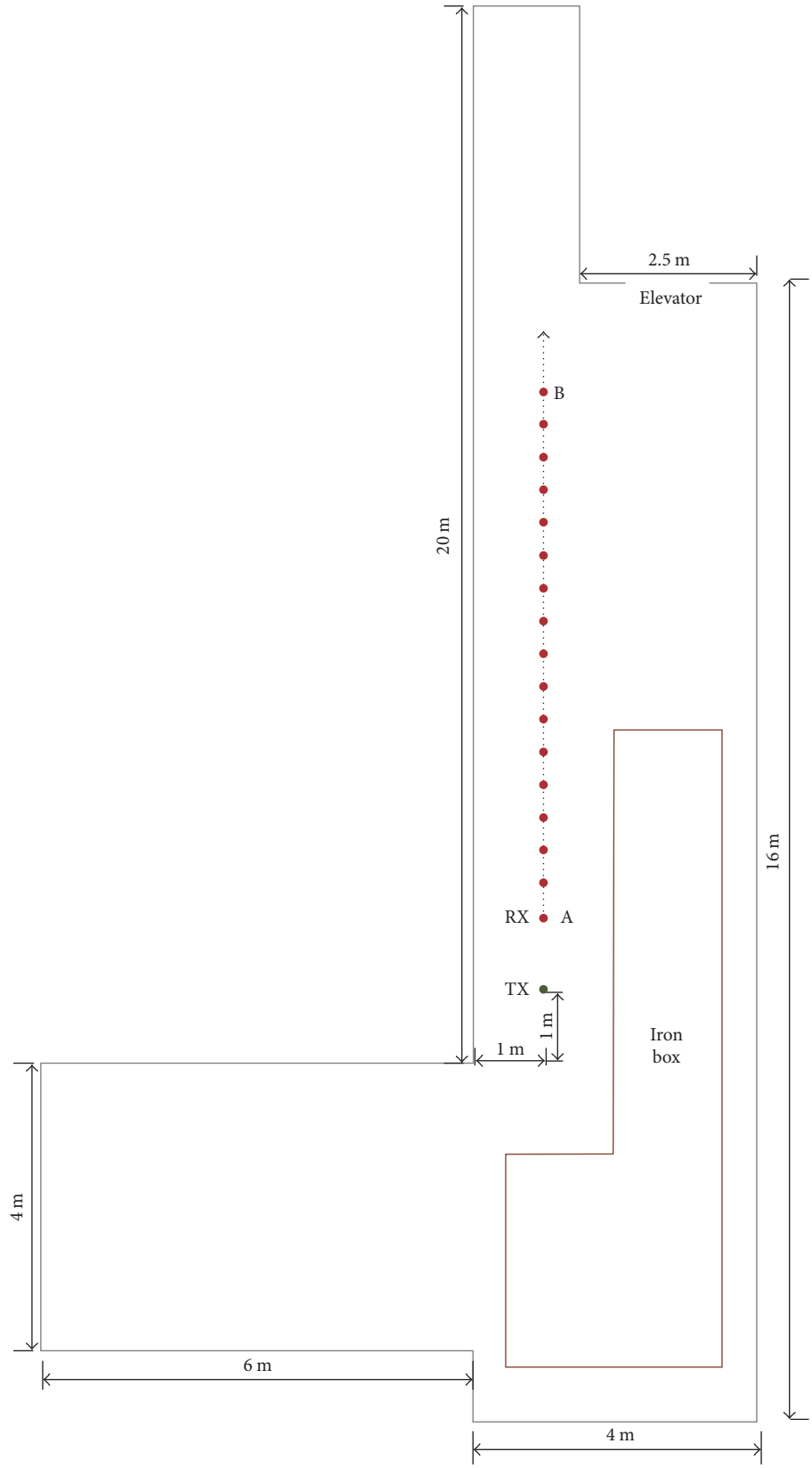

(d)

Figure 2: Measurement environment. (a) Photo of tunnel scenario 1, (b) photo of tunnel scenario 2, (c) sketched plan of tunnel scenario 1, and (d) sketched plan of tunnel scenario 2.

When used at a single frequency, the ABG model reverts to the existing 3GPP floating-intercept (FI) model with three parameters where γ set to 0 or 2 [5, 23]. Moreover, to verify the model accuracy, we use the simulated channel parameters to compare them with that of measured results.

Different path loss models have been deduced based on extensive wideband measurements at 6 GHz in terms of LOS and NLOS scenarios. Figures 3(a), 3(b), 3(c), and 3(d) show the scatter plots of all measured and simulated path loss values in dB versus TX-RX separation distance optimized for the CI, CI-opt, and ABG models in both LOS and NLOS environments. As a reference, free-space path loss models are also included. Table 2 summarizes the parameters of path loss models including measured results and simulated results for all scenarios including ABG models and CI models which consist of 1 m CI models and optimized d_0 models (CI-opt models).

From Figure 3, we can see that the values of path loss increase with increasing distance between transmitter and receiver. From Table 2, we can also see that the measured PLEs of CI are 1.72, 1.69, and 1.58 for LOS-1, LOS-2, and LOS-3 paths, respectively. Also, the simulated PLEs of CI are 1.66, 1.50, and 1.74, respectively. The measured PLEs of CI-opt are 1.75, 1.45, and 1.45, respectively. Furthermore, the simulated PLEs of CI-opt are 1.61, 1.55, and 1.71, respectively. The values of PLE are identical for measured CI-opt models in both LOS-2 and LOS-3 paths. These results indicate that the values of PLE are less than the free-space PLE ($n = 2$), implying that the multipath components (MPCs) from both side walls and floor add up constructively in the tunnel environments, as a guided wave phenomenon. It is seen that the measured PLE and simulated PLE of CI models are 2.18 and 2.20 for NLOS paths, respectively. Also, the measured PLE and simulated PLE of CI-opt models are 2.41 and 2.11 for NLOS paths, respectively, indicating faster signal level degradation over the distance between transmitter and receiver. Obvious explanation for this is that there are different dominating propagation mechanisms due to different structures of the tunnel scenarios. As indicated in Table 2, the standard deviations for CI models vary between 0.53 dB and 3 dB for LOS paths and the standard deviations for CI models vary between 2.74 dB and 4.2 dB for NLOS paths. Also, the standard deviations for CI-opt models vary between 0.38 dB and 2.10 dB for LOS paths and the standard deviations for CI models vary between 1.38 dB and 2.74 dB for NLOS paths. It is interesting to note that the difference of standard deviations for CI-opt models and CI models is always less than 1 dB for majority measurement and simulation sets, which demonstrate that there is no essential difference in standard deviations between CI models and CI-opt models. However, the standard deviations for ABG models vary between 1.06 dB and 8.27 dB for LOS paths and the standard deviations for ABG models vary between 7.41 dB and 7.68 dB for NLOS paths. It is worth noting that the difference of standard deviations for ABG models and CI models is always larger than 1 dB for majority measurement and simulation datasets indicating the higher accuracy and reliability of CI models compared to ABG models.

From these analyses, we can conclude that CI model with the reference distance of 1 m provides more accuracy and stability in LOS and NLOS tunnel scenarios at 6 GHz. These simulated results are in agreement with previous works [15, 16, 22, 32, 43, 44] which indicate that the path loss is best modeled by a log-distance relationship.

3.2. Received Power Results and Analysis. In wireless communication channels, the signal is transmitted and then undergoes direct reflection, transmission, scattering, and diffraction. Hence, the signal arriving at the receiver is the superposition of the various multipath components [45]. All cumulative distribution functions (CDF) of received power including measured results and simulated results are demonstrated for LOS and NLOS as shown in Figure 4. In both LOS and NLOS tunnel scenarios, the ray-tracing predictions agree fairly well with the measured results. There are slight differences between measured and simulated results as shown in Figure 4. They could be attributed to scattering by small objects within the tunnel scenarios and are not expected to influence the performance of wireless communication system. Moreover, the statistical method to determine the distribution of the CDF of received power after regression analysis is needed. Notice that the CDF is close to a normal distribution. The parameters of the distribution are listed in Table 3. μ and σ denote the mean and standard deviations of the normal distribution, respectively.

3.3. Statistical Analysis of RMS Delay Spreads. The mean excess delay and root-mean-square (RMS) delay are two important parameters used to characterize the temporal dispersive properties of multipath channels. The mean excess delay τ_{m} is defined as the first moment of the power delay profile (PDP) [46].

$$\tau_{\mathrm{m}} = \frac{\sum_k a_k^2 \tau_k}{\sum_k a_k^2} = \frac{\sum_k P(\tau_k)\tau_k}{\sum_k P(\tau_k)}, \tag{3}$$

where a_k, τ_k, and $P(\tau_k)$ are the gain coefficient delay and PDP of the kth MPC, respectively. The RMS delay spread (τ_{rms}) is the square root of the second central moment of the PDP and is defined to be

$$\tau_{\mathrm{rms}} = \sqrt{\tau_{\mathrm{m}}^2 - (\tau_{\mathrm{m}})^2}, \tag{4}$$

where

$$\tau_{\mathrm{m}}^2 = \frac{\sum_k a_k^2 \tau_k^2}{\sum_k a_k^2} = \frac{\sum_k P(\tau_k)\tau_k^2}{\sum_k P(\tau_k)}. \tag{5}$$

The RMS delay spread for LOS-2, LOS-3, and NLOS paths is shown in Figure 5. The RMS delay spread values vary between 2.77 and 18.76 ns. From Figure 5, we can see that the correlation between RMS delay spread and the distance between transmitter and receiver is very low. Also, it is seen that the RMS delay spread values in LOS paths are lower than the values in NLOS path due to the difference of structure of tunnel and the small scattering objects. In fact, the presence of obstructions in tunnel environment (compared with the

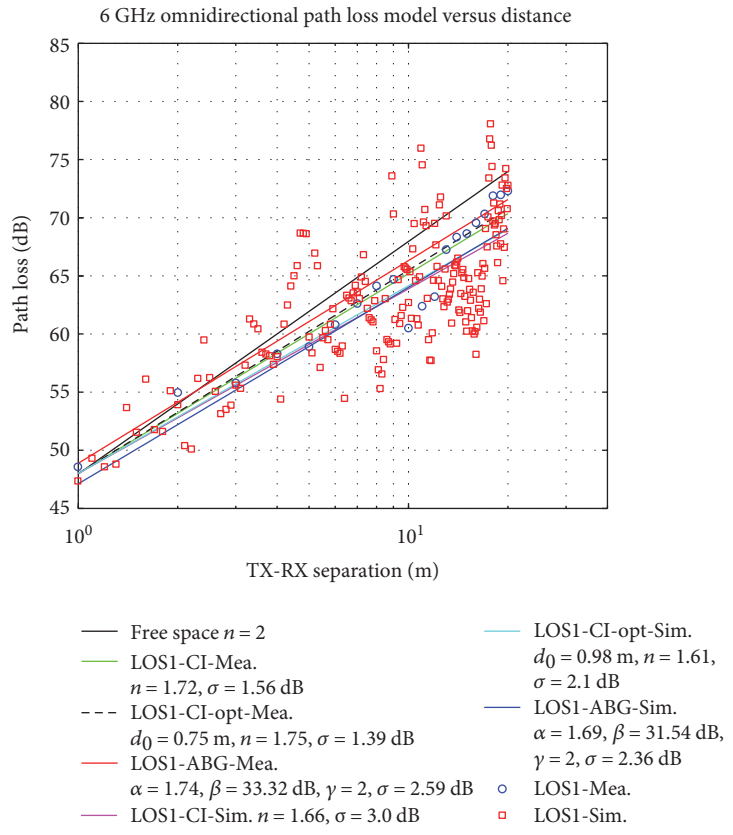

(a)

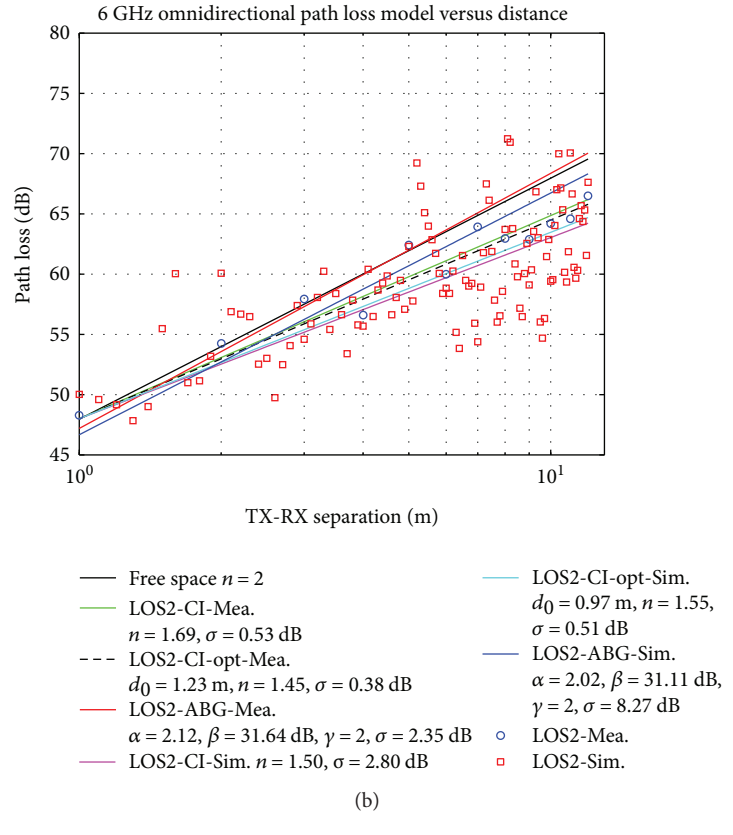

(b)

Figure 3: Continued.

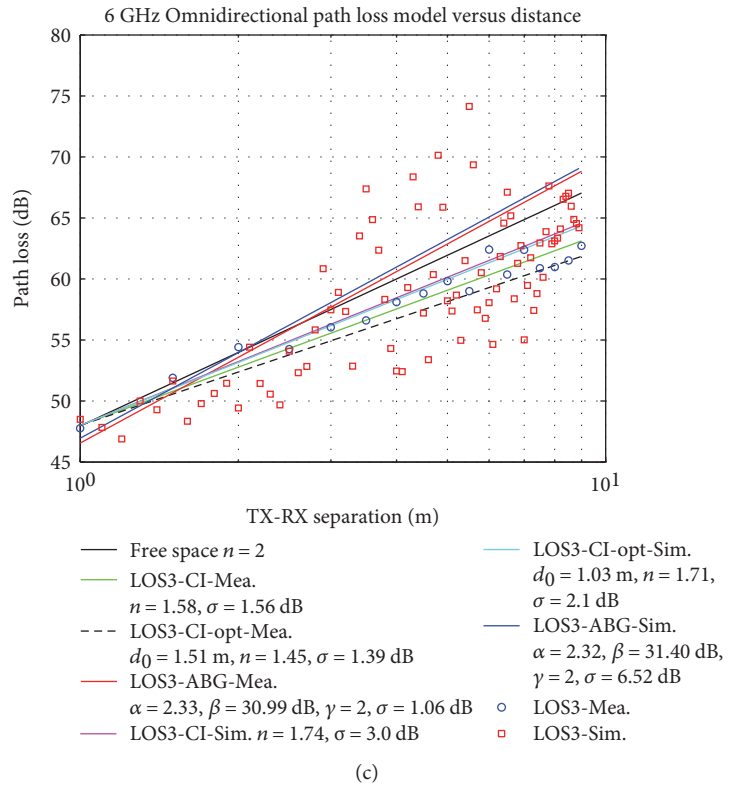

(c)

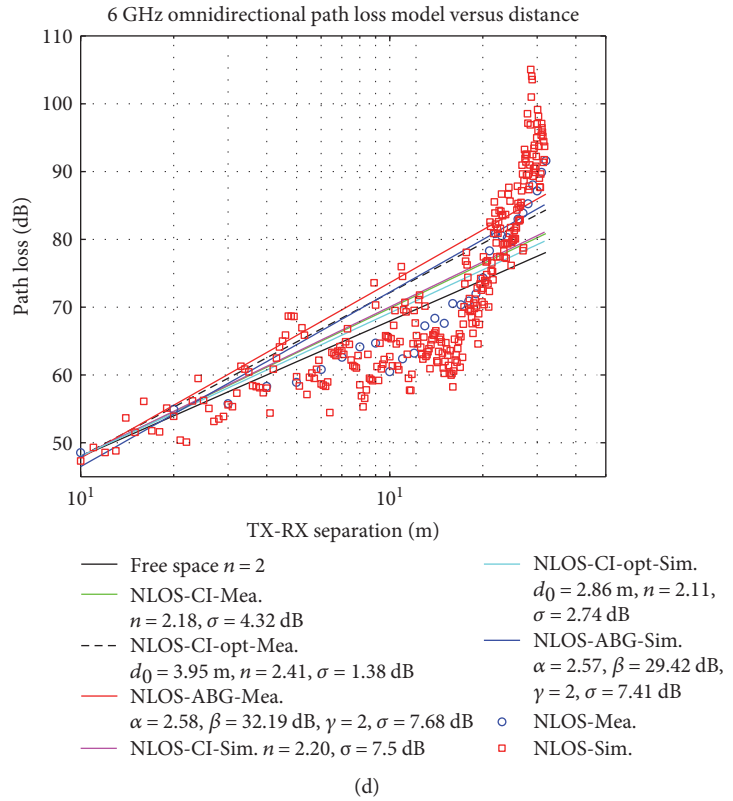

(d)

Figure 3: Path loss variation with TX-RX separation distance using CI and ABG models. (a) LOS-1 path in tunnel scenario-1, (b) LOS-2 path in tunnel scenario 1, (c) LOS-3 path in tunnel scenario 2, and (d) NLOS path in tunnel scenario 1.

equivalent empty room) has inconsistent effects on the multipath [47]. Moreover, RMS delay spread increases when reflections and scattering induce larger propagation delay times in wireless channel. Figures 6(a), 6(b), 6(c), and 6(d) show the empirical CDFs of RMS delay spreads for all scenarios, which include the Poisson, Exponential, Rayleigh, and

Table 2: Parameters in the ABG, CI, and CI-opt path loss models in tunnel scenarios in terms of LOS and NLOS paths at 6 GHz. Dis. Ran. denotes distance range. Number of data points denotes the number of data points.

Sce.	Env.		Number of data points	Dis. Ran. (m)	ABG				CI		CI-opt		
					α	β (dB)	γ	σ (dB)	n	σ (dB)	d_0 (m)	n	σ (dB)
Tunnel 1	LOS-1	Mea.	20	21	1.74	33.32	2	2.59	1.72	1.56	0.75	1.75	1.39
		Sim.	191	21	1.69	31.54	2	2.36	1.66	3.00	0.98	1.61	2.10
	LOS-2	Mea.	12	13	2.12	31.64	2	2.35	1.69	0.53	1.23	1.45	0.38
		Sim.	111	13	2.02	31.11	2	8.27	1.50	2.80	0.97	1.55	0.51
	NLOS	Mea.	32	33	2.58	32.19	2	7.68	2.18	4.32	3.95	2.41	1.38
		Sim.	308	33	2.57	29.42	2	7.41	2.20	7.50	2.86	2.11	2.74
Tunnel 2	LOS-3	Mea.	17	18	2.33	30.99	2	1.06	1.58	1.56	1.51	1.45	1.39
		Sim.	80	18	2.32	31.40	2	6.52	1.74	3.00	1.03	1.71	2.10

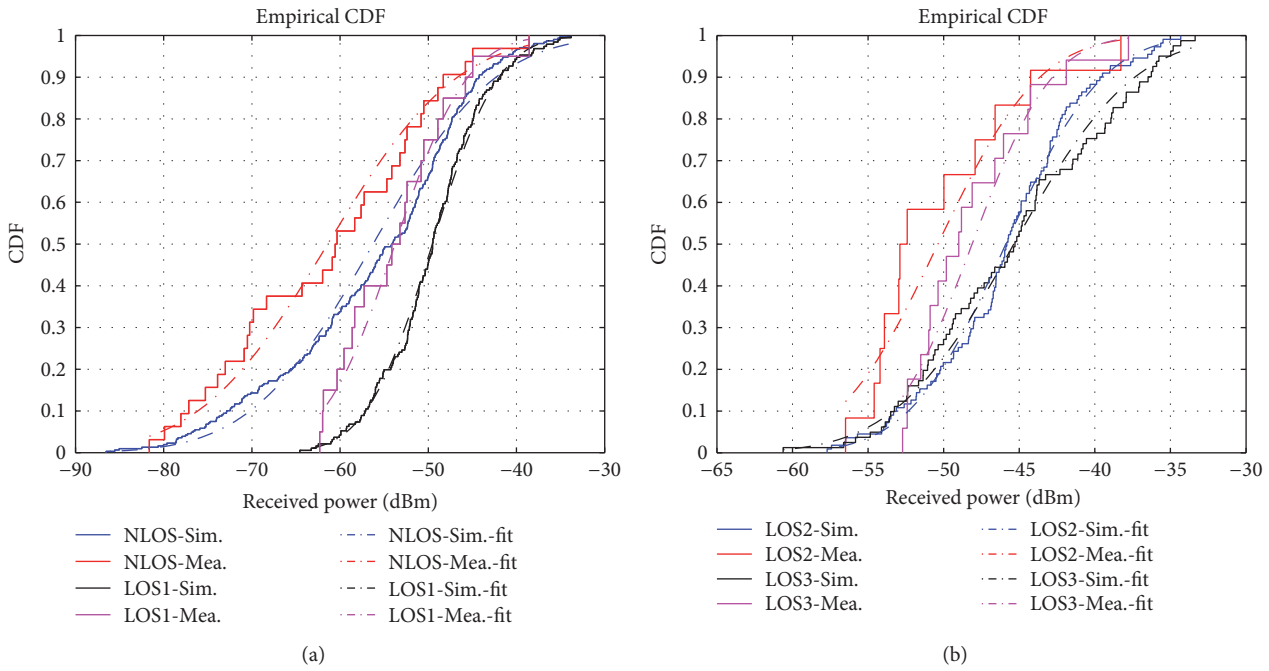

Figure 4: Cumulative distribution function (CDF) of the received power at 6 GHz in LOS and NLOS tunnel scenarios. (a) LOS-1 and NLOS paths and (b) LOS-2 and LOS-3 paths.

Table 3: Received power values for all scenarios.

Scenarios			Fitted parameters				
			μ (dB)	σ (dB)	Max (dB)	Min (dB)	Median (dB)
Tunnel 1	LOS-1	Mea.	−53.76	6.45	−38.55	−62.31	−53.68
		Sim.	−49.53	5.90	−33.80	−64.56	−49.51
	LOS-2	Mea.	−45.36	6.24	−33.37	−60.62	−45.28
		Sim.	−45.89	5.03	−34.32	−57.71	−45.82
	NLOS	Mea.	−61.4	11.49	−38.55	−81.62	−60.44
		Sim.	−56.25	10.88	−33.80	−86.13	−54.10
Tunnel 2	LOS-3	Mea.	−48.12	4.15	−37.78	−52.71	−48.99
		Sim.	−50.38	5.26	−38.28	−56.49	−52.65

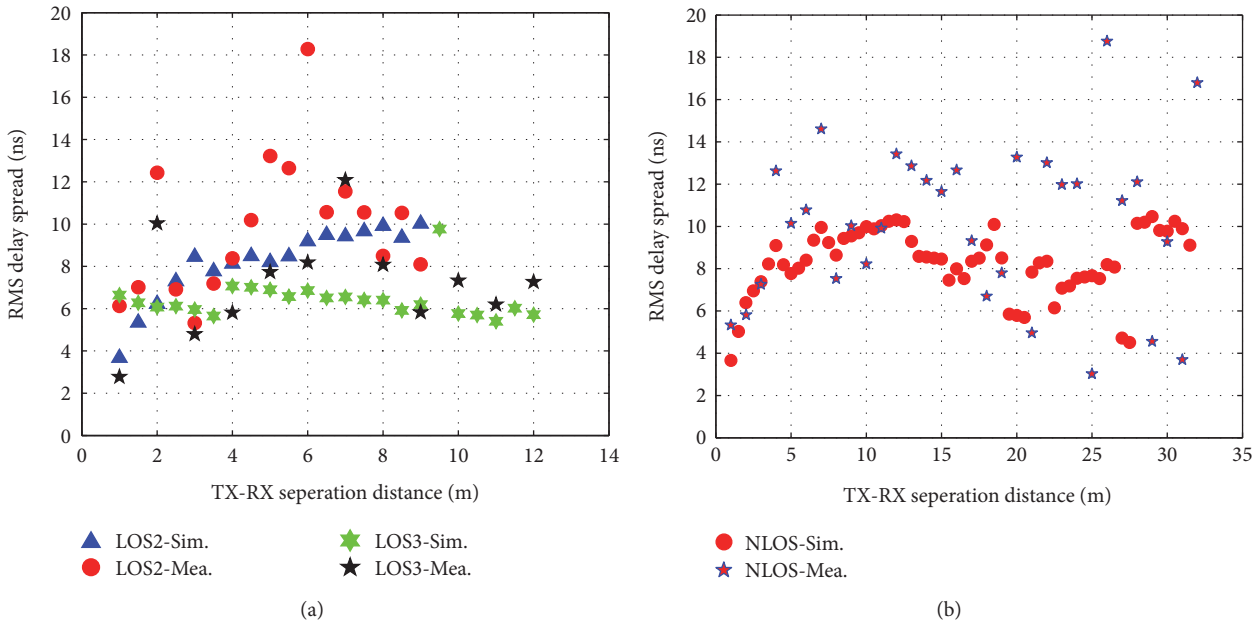

Figure 5: RMS delay spread variation with TX-RX separation distance in LOS and NLOS tunnel scenarios. (a) LOS-2 and LOS-3 paths and (b) NLOS path.

Gaussian distribution. In order to identify the distribution, the Log-likelihood test is adopted. After estimating the maximum likelihood of the distribution parameters, it is, therefore, evident that the Poisson distribution best fits the measured data of RMS delay spreads for LOS scenarios and the Gaussian distribution best fits the measured data of RMS delay spreads for NLOS scenarios as shown in Figure 6. Moreover, it is apparent that 90% of the energy arrived at the RX within 13.2 ns for LOS scenarios and 14.6 ns for NLOS scenarios. The mean, minimum, and maximum of RMS delay spreads are listed in Table 4 for all tunnel environments.

3.4. Ricean K-Factor Analysis. K-factor is a significant parameter in wireless communications because it is able to characterize the type of fading environments [48]. Ricean K-factor is the power ratio between the LOS component and the sum of other propagation components [42]. K-factor can be calculated as

$$K = \frac{P_k(\max)}{\sum_k [P_k - P_k(\max)]}, \tag{6}$$

where $P_k(\max)$ is the maximum power for LOS path and P_k is the total power for all paths.

Ricean K-factor (KF) values at different distances between transmitter and receiver for LOS paths are shown in Figure 7. The maximum K-factor for LOS-1 is 12.67 dB, and the mean is 7.67 dB. Specially, the maximum K-factor for LOS-3 is 11.21 dB and the mean is 6.73 dB which are consistent to the values for LOS-1. However, it is seen that the maximum K-factor for LOS-2 is 18.30 dB and the mean is 9.61 dB, which are larger than the values of LOS-1. The difference between them is mainly because tunnel 1 and tunnel 3 are straight tunnel and tunnel 2 is curved tunnel which may result in fewer multipath components. It is seen that the correlation is low between Ricean K-factor and the distance between transmitter and receiver. Moreover, the CDF plots of K-factor are shown in Figure 8. The results lead to an observation that the normal distribution provides good fits to the Ricean K-factor for LOS tunnel scenarios. The statistical parameters for K-factor (expressed in dB) are shown below:

$$\mathrm{KF} = \sim N[\mu_{\mathrm{dB}}, \sigma_{\mathrm{dB}}] \sim \begin{cases} N\left[7.67, 2.62^2\right], & \text{for LOS} - 1 \\ N\left[9.61, 3.96^2\right], & \text{for LOS} - 2 \\ N\left[6.73, 2.65^2\right], & \text{for LOS} - 3. \end{cases} \tag{7}$$

3.5. AOA Analysis. The angles θ_A and φ_A with reference to the spherical coordinate system give the direction from which the propagation path arrives at receiver point. The mean angle of arrival from which energy arrives at the receiver is defined as

$$\bar{\theta}_A = \tan^{-1}\left(\frac{\sqrt{A_x^2 + A_y^2}}{A_z}\right) \quad \bar{\phi}_A = \cos^{-1}\left(\frac{A_y}{A_x}\right),$$
$$A = \sum_{i=1}^{N_p} P_i \overrightarrow{a_i},$$
$$\overrightarrow{a_i} = \sin(\theta_A)\cos(\phi_A)\,\overrightarrow{x} + \sin(\theta_A)\sin(\phi_A)\,\overrightarrow{y} + \cos(\theta_A)\,\overrightarrow{z}, \tag{8}$$

where P_i is the power carried by ith path and $\overrightarrow{a_i}$ is the unit vector in the direction from which the ith path arrives at the receiver.

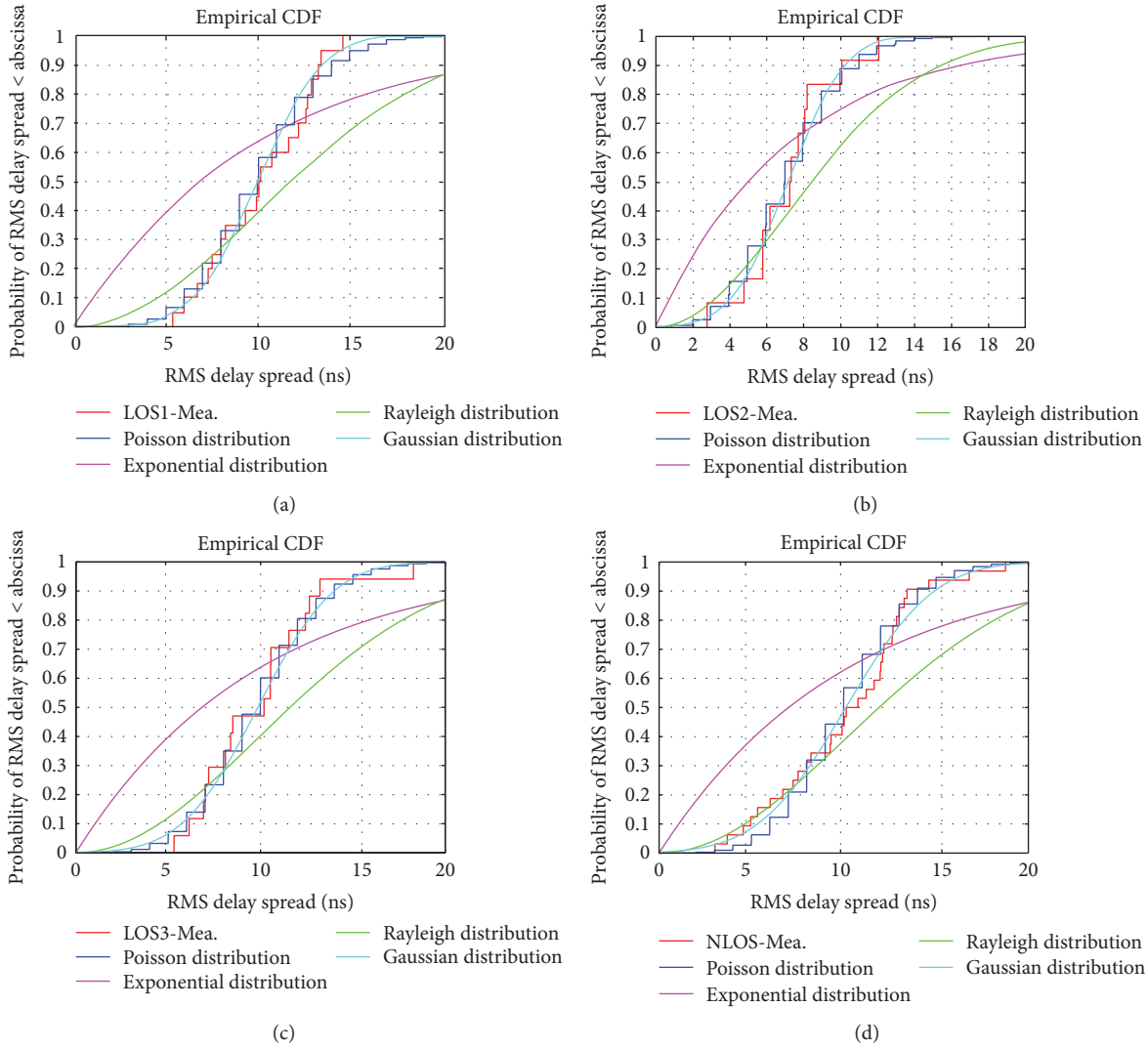

Figure 6: CDF for RMS delay spreads at 6 GHz in LOS and NLOS tunnel scenarios. (a) LOS-1 path, (b) LOS-2 path, (c) LOS-3 path, and (d) NLOS path.

Table 4: RMS delay spread values for all scenarios.

Scenarios			Fitted parameters				
			μ (ns)	σ (ns)	Max (ns)	Min (ns)	Median (ns)
Tunnel 1	LOS-1	Mea.	10.01	2.75	14.61	5.34	10.08
		Sim.	8.42	1.51	10.31	3.66	8.51
	LOS-2	Mea.	5.41	0.86	8.76	4.40	5.28
		Sim.	7.18	2.41	12.09	2.77	2.41
	NLOS	Mea.	10.12	3.74	18.76	3.03	10.46
		Sim.	8.30	1.59	10.46	3.66	8.43
Tunnel 2	LOS-3	Mea.	9.85	3.23	18.28	5.32	3.23
		Sim.	8.18	1.73	10.02	3.67	8.48

In terms of the angle of arrival, some conclusions are presented. The distribution of AOA in the elevation plane has been researched [49, 50]. The distribution of AOA in the elevation plane is described as Gaussian [49] and uniform [50]. However, there are few reports on the characteristics of distribution of AOA at 6 GHz. The CDF distributions of mean AOA are shown in Figure 9. From Figure 9, we can see that the normal distribution provides good fits to the mean AOA for LOS-1, LOS-3, and NLOS paths. Moreover, the best distribution that fits the measured data is the

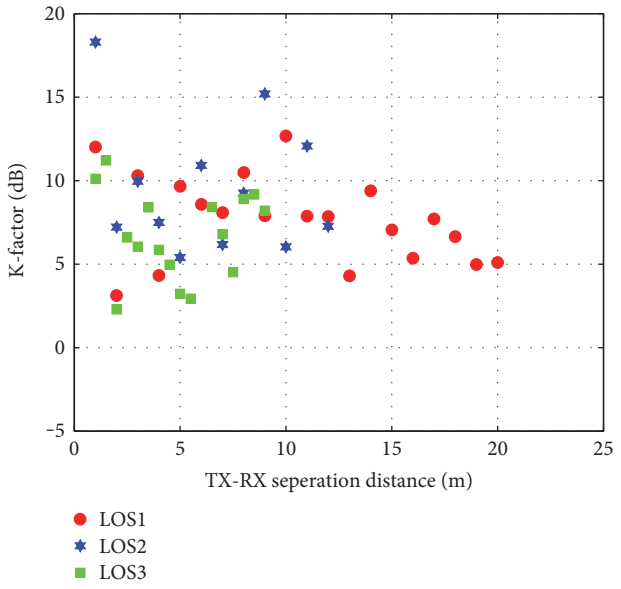

Figure 7: Rician K-factor variation with TX-RX separation distance in LOS tunnel scenarios.

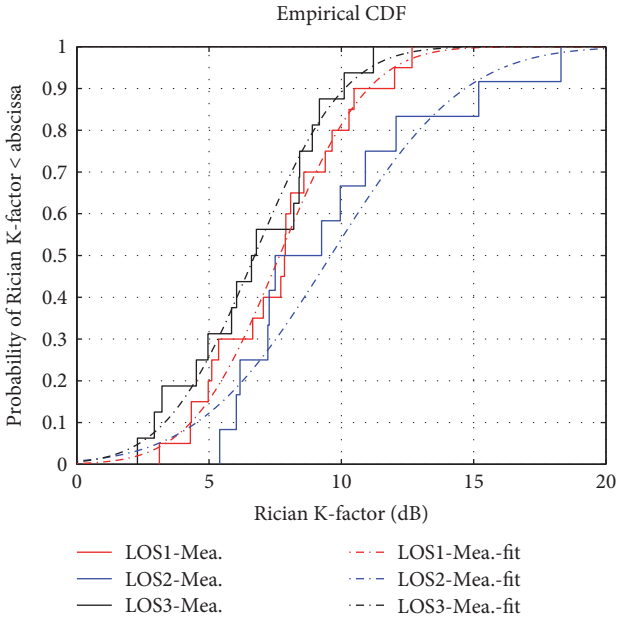

Figure 8: CDF for Rician K-factor in LOS tunnel scenarios.

uniform distribution in LOS-2 as depicted in Figure 9. These results are in agreement with previous works. The statistical parameters for mean AOA are shown below

$$\text{AOA} = \sim \begin{cases} N\left[167^\circ, (86^\circ)^2\right], & \text{for NLOS} \\ N\left[159^\circ, (74^\circ)^2\right], & \text{for LOS-1} \\ U[0^\circ, 360^\circ], & \text{for LOS-2} \\ N\left[161^\circ, (44^\circ)^2\right], & \text{for LOS-3.} \end{cases} \quad (9)$$

In addition, some important arrival angles are extracted based on subtractive clustering algorithm [51] as shown in

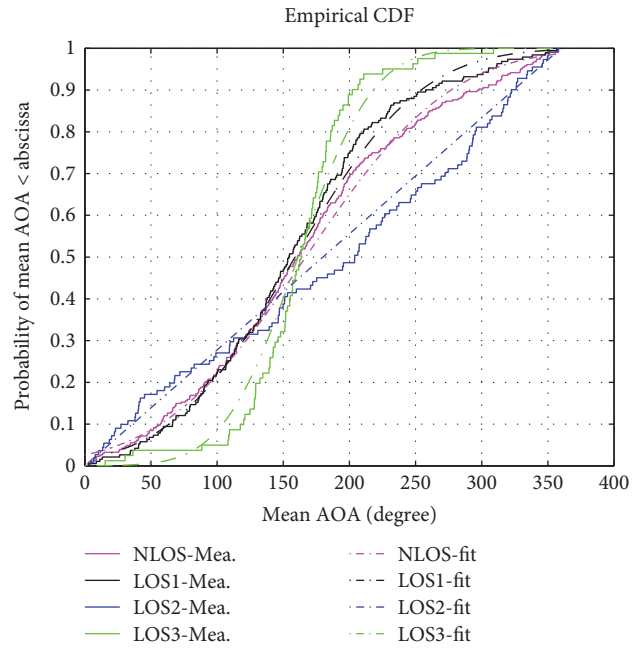

Figure 9: CDF for mean AOA in tunnel scenarios.

Figures 10(a), 10(b), 10(c), and 10(d). Furthermore, the extracted parameters of AOA are listed in Table 5. These parameters presented here can be used for wireless communication system design in indoor environments and can be used for adaptive transmission technologies for 5G wireless network.

4. Conclusion

In this paper, extensive measurements and characterizations of wideband tunnel channel have been proposed. Channel characteristics such as path loss models, received power, RMS delay spread, Ricean K-factor, and AOA are described and modeled. Based on extensive radio channel sounding campaigns and simulations, it is found that the ray-tracing predictions agree fairly well with the measured results. Comparison with path loss models illustrates the fact that the CI model with the reference distance of 1 m was shown to be the most suitable because of its accuracy and simplicity in tunnel scenarios. The CI path loss models indicated that the PLEs vary between 1.50 and 1.74 in LOS scenarios and between 2.18 and 2.20 in NLOS scenarios. The CDF of received power follows the normal distribution. The normal distribution provides good fits to the Ricean K-factor for LOS scenarios. The Poisson distribution model best fits the measured data of RMS delay spreads for LOS scenarios, and the Gaussian distribution model best fits the measured data of RMS delay spreads for NLOS scenarios. Moreover, the normal distribution and the uniform distribution reasonably fit the AOA well for all tunnel scenarios. In addition, propagation characteristics with the effects of human movement and vehicular motion on wireless channels require further measurement and analysis in the complex environments, which is the next research direction.

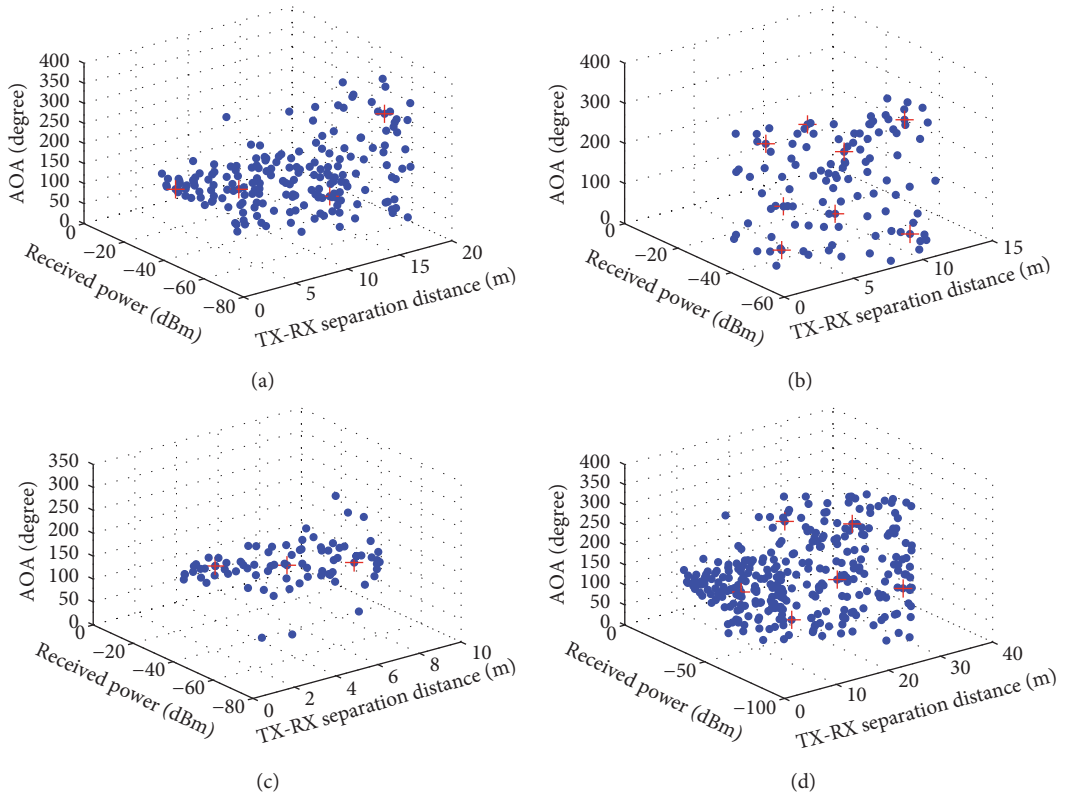

Figure 10: Mean AOA in tunnel scenarios. (a) LOS-1 path, (b) LOS-2 path, (c) LOS-3 path, and (d) NLOS path.

Table 5: AOA parameters for all scenarios.

Scenarios		Cluster parameters		
		TX-RX (m)	Received power (dBm)	AOA (degree)
Tunnel 1	LOS1	1.50	−38.03	162
		5.80	−47.32	153
		13.70	−51.68	90
		18.50	−54.05	267
	LOS2	2.70	−38.97	292
		2.90	−43.87	40
		3.40	−41.89	139
		6.20	−46.73	109
		7.10	−45.40	251
		10.30	−53.49	41
		10.90	−48.34	304
	NLOS	4.40	−45.74	345
		7.70	−47.70	142
		15.30	−50.32	296
		16.60	−50.37	47
		22.10	−60.96	147
		23.70	−65.14	288
		30.40	−75.21	122
Tunnel 2	LOS3	2.30	−37.04	174
		5.10	−43.85	155
		7.70	−50.36	142

Conflicts of Interest

The authors declare that they have no conflicts of interest.

Acknowledgments

This work has been supported by the National Natural Science Fund under Grant no. 61372045 and by the Postgraduate Research & Practice Innovation Program of Jiangsu Province in 2016 under Grant no. KYLX16_0650. The work of this paper is funded by Radio Wave Environment Characteristics and Modeling Technology Key Laboratory under Grant no. 201600013. Moreover, the authors would like to thank Dr. R. C. Sun, Q. C. Li, Y. Lei, and Y. H. Wu for their help with the measurements and associate Professor L. Liu from Institute of Broadband Wireless Mobile Communications at Beijing Jiaotong University, Beijing, for providing radio propagation measurement equipment used for preliminary measurements.

References

[1] M. K. Samimi and T. S. Rappaport, "3-D millimeter-wave statistical channel model for 5G wireless system design," *IEEE Transactions on Microwave Theory and Techniques*, vol. 64, pp. 2207–2225, 2016.

[2] Millimeter-wave Based Mobile Radio Access Network for 5G Integrated Communications (mmMagic), "Use case characterization, KPIs and preferred suitable frequency ranges for future 5G systems between 6 GHz and 100 GHz," August 2016, http://5g-mmmagic.eu/results/.

[3] A. M. Al-Samman, T. A. Rahman, M. H. Azmi, M. N. Hindia, I. Khan, and E. Hanafi, "Statistical modeling and characterization of experimental mm-wave indoor channels for future 5G wireless communication networks," *PLoS One*, vol. 11, pp. 1–29, 2016.

[4] Z. Y. Pi and F. Khan, "An introduction to millimeter-wave mobile broadband systems," *IEEE Communication Magazine*, vol. 49, pp. 101–107, 2011.

[5] T. S. Rappaport, G. R. MacCartney Jr., M. K. Samimi, and S. Sun, "Wideband millimeter-wave propagation measurements and channel models for future wireless communication system design," *IEEE Transactions on Communications*, vol. 63, pp. 3029–3056, 2015.

[6] A. Ghosh, T. A. Thomas, M. C. Cudak et al., "Millimeter-wave enhanced local area systems: a high-data-rate approach for future wireless networks," *IEEE Journal on Selected Areas in Communications*, vol. 32, pp. 1152–1163, 2014.

[7] International Telecommunication Union Radiocommunication Sector (ITU-R), "Future spectrum requirements estimate for terrestrial IMT report ITU-R M.2290-0," August 2016, http://www.itu.int/pub/R-REP-M.2290-2014.

[8] Mobile and Wireless Communications Enablers for the Twenty-twenty Information Society (METIS), "Initial channel models based on measurements," D1.2, http://www.metis2020.com.

[9] G. R. MacCartney Jr., T. S. Rappaport, S. Sun, and S. J. Deng, "Indoor office wideband millimeter-wave propagation measurements and channel models at 28 and 73 GHz for ultra-dense 5G wireless networks," *IEEE Access*, vol. 3, pp. 2388–2424, 2015.

[10] T. S. Rappaport, S. Sun, R. Mayzus et al., "Millimeter-wave mobile communications for 5G cellular: it will work!," *IEEE Access*, vol. 1, pp. 335–349, 2013.

[11] Millimeter-wave Evolution for Backhaul and Access (MiWEBA), "Channel modeling and characterization," D5.1, http://www.miweba.eu.

[12] Millimeter-wave Based Mobile Radio Access Network for 5G Integrated Communications (mmMagic), "Channel measurements and modeling," WP2, http://5g-mmmagic.eu.

[13] M. Peter, R. J. Weiler, W. Keusgen, T. Eichler, M. Kottkamp, and A. Nahring, "Characterization of mm-wave channel sounders up to W-band and validation of measurement results," in *2016 IEEE 10th European Conference on Antennas and Propagation (EuCAP)*, pp. 1–5, Davos, Switzerland, 2016.

[14] J. Blumenstein, T. Mikulasek, T. Zemen, C. Mecklenbrauker, R. Marsalek, and A. Prokes, "In-vehicle mm-wave channel model and measurement," in *2014 IEEE 80th Vehicular Technology Conference (VTC Fall)*, pp. 1–5, Vancouver, BC, Canada, 2014.

[15] J. Kivinen, X. W. Zhao, and P. Vainikainen, "Empirical characterization of wideband indoor radio channel at 5.3GHz," *IEEE Transactions on Antennas and Propagation*, vol. 49, pp. 1192–1203, 2001.

[16] M. Peter, R. J. Weiler, B. Goktepe, W. Keusgen, and K. Sakaguchi, "Channel measurement and modeling for 5G urban microcellular scenarios," *Sensors*, vol. 16, p. 1330, 2016.

[17] M. Kim, J. I. Takada, Y. Y. Chang, J. Y. Shen, and Y. Oda, "Large scale characteristics of urban cellular wideband channels at 11 GHz," in *2015 IEEE 9th European Conference on Antennas and Propagation (EuCAP)*, pp. 1–4, Lisbon, Portugal, 2015.

[18] J. Vehmas, J. Jarvelainen, S. L. H. Nguyen, R. Naderpour, and K. Haneda, "Millimeter-wave channel characterization at Helsinki airport in the 15, 28, and 60 GHz bands," in *2016 IEEE 84th Vehicular Technology Conference (VTC-Fall)*, pp. 1–5, Montreal, QC, Canada, 2016.

[19] T. S. Rappaport, "Multi-beam antenna combing for 28 GHz cellular link improvement in urban environments," in *2013 IEEE Global Communications Conference (GLOBECOM)*, pp. 3754–3759, Atlanta, GA, USA, 2013.

[20] S. Hur, Y. J. Cho, T. Kim et al., "Wideband spatial channel model in an urban cellular environments at 28 GHz," in *2015 IEEE 9th European Conference on Antennas and Propagation (EuCAP)*, pp. 1–5, Lisbon, Portugal, 2015.

[21] Y. P. Zhu, H. M. Wang, W. Hong, J. W. Dou, S. P. Mei, and X. Yuan, "28-GHz path-loss measurement and modeling in indoor environments," in *2015 IEEE 6th International Symposium on Microwave, Antenna, Propagation, and EMC Technologies (MAPE)*, pp. 234–237, 2015.

[22] X. W. Zhao, S. Li, Q. Wang, M. J. Wang, S. H. Sun, and W. Hong, "Channel measurements, modeling, simulation and validation at 32 GHz in outdoor microcells for 5G radio systems," *IEEE Access*, vol. 5, pp. 1062–1072, 2016.

[23] G. R. MacCartney, J. H. Zhang, S. Nie, and T. S. Rappaport, "Path loss models for 5G millimeter wave propagation channels in urban microcells," in *2013 IEEE Global Communications Conference (GLOBECOM)*, pp. 3948–3953, Atlanta, GA, USA, 2013.

[24] S. Sun, T. S. Rappaport, T. A. Thomas et al., "Investigation of prediction accuracy, sensitivity, and parameter stability of large-scale propagation path loss models for 5G wireless communications," *IEEE Transactions on Vehicular Technology*, vol. 65, pp. 2843–2860, 2016.

[25] J. Ryan, G. R. MacCartney Jr., and T. S. Rappaport, "Indoor office wideband penetration loss measurements at 73 GHz," in *2017 IEEE International Conference on Communications Workshop (ICC Workshops)*, pp. 1–6, Paris, France, 2017.

[26] G. R. MacCartney Jr., H. S. Yan, S. Sun, and T. S. Rappaport, "A flexible wideband millimeter-wave channel sounder with local area and NLOS to LOS transition measurements," in *IEEE International Conference on Communications (ICC)*, pp. 1–7, Paris, France, 2017.

[27] N. Moraitis and P. Constantinou, "Measurements and characterization of wideband indoor radio channel at 60 GHz," *IEEE Transactions Wireless Communications*, vol. 5, pp. 880–889, 2006.

[28] P. F. M. Smulders, "Statistical characterization of 60-GHz indoor radio channels," *IEEE Transactions on Antennas and Propagation*, vol. 57, pp. 2820–2829, 2009.

[29] M. Z. Zaaimia, R. Touhami, L. Talbi, M. Nedil, and M. C. E. Yagoub, "60-GHz statistical channel characterization for wireless data centers," *IEEE Antennas and Wireless Propagation Letters*, vol. 15, pp. 976–979, 2016.

[30] K. Haneda, J. Jarvelainen, A. Karttunen, M. Kyro, and J. Putkonen, "A statistical spatio-temporal radio channel model for large indoor environments at 60 and 70 GHz," *IEEE Transactions on Antennas and Propagation*, vol. 63, pp. 2694–2704, 2015.

[31] P. B. Papazian, C. Gentile, K. A. Remley, J. Senic, and N. Golmie, "A radio channel sounder for mobile millimeter-wave communications: system implementation and measurement assessment," *IEEE Transactions on Microwave Theory and Techniques*, vol. 64, pp. 2924–2932, 2016.

[32] M. Jacob and T. Kurner, "Radio channel characteristics for broadband WLAN/WPAN applications between 67 and 110 GHz," in *2009 IEEE 3rd European Conference on Antennas and Propagation 2009 EuCAP*, pp. 2663–2667, Berlin, Germany, 2009.

[33] S. H. Chen and S. K. Jeng, "An SBR/image approach for radio wave propagation in indoor environments with metallic furniture," *IEEE Transactions on Antennas and Propogation*, vol. 45, pp. 98–106, 1997.

[34] J. C. Xiao, C. Tao, L. Liu, Y. P. Lu, W. J. Li, and P. Y. Liu, "Development of virtual massive MIMO channel measurement system," *Journal of Electronic Measurement and Instrumentation*, vol. 30, pp. 101–110, 2016.

[35] Remcom, *Wireless Insite Reference Manual, Ver.2.8.1*, 2016.

[36] International Telecommunication Union Radiocommunication Sector (ITU-R), "Effects of building materials and structures on radiowave propagation above 100 MHz report ITU-R P.2040," 2013.

[37] I. Cuinas, J. P. Pugliese, A. Hammoudeh, and M. G. Sanchez, "Comparison of the electromagnetic properties of building materials at 5.8 GHz and 62.4 GHz," in *2000 IEEE 52nd Vehicular Technology Conference*, vol. 2, pp. 780–785, Boston, MA, USA, 2000.

[38] L. M. Correia and P. O. Frances, "Estimation of materials characteristics from power measurements at 60 GHz," *IEEE International Symposium on Personal, Indoor and Mobile Radio Communications*, vol. 2, pp. 510–513, 1994.

[39] M. Lott and I. Forkel, "A multi-wall-and-floor model for indoor radio propagation," in *2001 IEEE Vehicular 53rd VTS Technology Conference Spring 2001 VTC*, pp. 464–468, 2001.

[40] M. E. Azhari, M. Nedil, I. B. Mabrouk, and L. Talbi, "Path loss effect on off-body channel capacity of a MIMO system using patch antennas inside a mine," in *2016 IEEE International Symposium on Antennas and Propagation (APSURSI)*, pp. 1697-1698, Fajardo, Puerto Rico, 2016.

[41] International Telecommunication Union Radiocommunication Sector (ITU-R), "Guidelines for evaluation of radio interface technologies for IMT-advanced report ITU-R M. M.2135-1.

[42] B. M. Donlan, D. R. McKinstry, and R. M. Buehre, "The UWB indoor channel: large and small scale modeling," *IEEE Transactions on Wireless Communications*, vol. 5, pp. 2863–2873, 2006.

[43] X. W. Zhao, S. Y. Geng, and B. M. Coulibaly, "Path-loss model including LOS-NLOS transition regions for indoor corridors at 5 GHz," *IEEE Antennas and Propagation Magazine*, vol. 55, pp. 217–223, 2013.

[44] J. Medbo, P. Kyosti, K. Kusume et al., "Radio propagation modeling for 5G mobile and wireless communications," *IEEE Communications Magazine*, vol. 54, pp. 144–151, 2016.

[45] T. S. Rappaport, R. W. Heath Jr., R. C. Daniels, and J. N. Murdock, *Millimeter Wave Wireless Communications*, Person/Prentice Hall, 2015.

[46] T. S. Rappaport, *Wireless Communications, Principles and Practice*, Prentice Hall, 2nd ed edition, 2002.

[47] S. Collonge, G. Zaharia, and G. E. Zein, "Influence of furniture on 60GHz radio propagation in a residential environment," *Microwave and Optical Technology Letters*, vol. 39, pp. 230–233, 2003.

[48] V. A. Fono and L. Talbi, "Modeling the effect of periodic wall roughness on the indoor radio propagation channel," *Progress in Electromagnetics Research M*, vol. 49, pp. 167–179, 2016.

[49] T. Taga, "Analysis for mean effective gain of mobile antennas in land mobile radio environment," *IEEE Transactions on Vehicular Technology*, vol. 39, pp. 117–131, 1990.

[50] X. W. Zhao, J. Kivinen, P. Vainikainen, and K. Skog, "Characterization of doppler spectra for mobile communications at 5.3 GHz," *IEEE Transactions on Vehicular Technology*, vol. 52, pp. 14–23, 2003.

[51] M. H. Rezaeian, S. Esmaeili, and R. Fadaeinedjad, "Generator coherency and network partitioning for dynamic equivalencing using subtractive clustering algorithm," *IEEE Systems Journal*, vol. PP, pp. 1–11, 2017.